EES Catalysis

PAPER

View Article Online
View Journal

Cite this: DOI: 10.1039/d5ey00338e

Reaction network of CO_2 hydrogenation into C_{1-2} oxygenates and its BEP relationships

Mikhail V. Polynski and Sergey M. Kozlov *

Although copper is one of the most common components in catalysts for CO_2 conversion into valuable C_{2+} chemicals, a clear and systematic mechanistic explanation of its unique properties in these processes is lacking. Herein, we address this challenge by introducing a novel ansatz to rationally construct catalytic reaction networks and account for realistic active sites on catalyst nanoparticles, applied here to CO_2 hydrogenation into C_1 and C_2 oxygenates, explaining the formation of frequently observed reaction intermediates. We also provide a comparative mechanistic analysis of CO_2 hydrogenation on a stronger-adsorbing metal widely used in hydrogenation reactions, Pd. Furthermore, we present a refined approach to Brønsted–Evans–Polanyi relationships tailored to structural characteristics of transition states. Our approach facilitates further exploration of CO_2 hydrogenation on transition metal-based catalysts, deepening our understanding of the underlying reaction mechanism. This theoretical framework not only elucidates the intricate kinetics of CO_2 hydrogenation but also establishes a versatile foundation for rational catalyst design across catalytic domains. This study highlights the unique activity of Cu in various hydrogenation and C–C coupling steps. Unlike scarce metals that require resource-intensive extraction, Cu reduces the environmental impact and costs of CO_2 conversion technologies. Clarifying its unique role in converting CO_2 into valuable C_{2+} chemicals moves us closer to balancing economic growth and environmental protection.

Received 30th November 2025,
Accepted 20th January 2026

DOI: 10.1039/d5ey00338e

rsc.li/eescatalysis

Broader context

Balancing environmental protection with industrial growth is particularly critical today. The catalytic conversion of CO_2, the most abundant anthropogenic greenhouse gas, into fuels and commodity chemicals is a promising route to reconcile environmental and economic objectives. However, its large-scale deployment is still hindered by complex reaction networks and the need for efficient yet earth-abundant catalysts. Here, we address these challenges by developing a computational framework that maps CO_2 hydrogenation pathways to C_{1-2} oxygenates on Cu-based nanoparticle catalysts, treating facets and edges as integrated active sites and accounting for co-adsorption and nanostructuring effects. Our rational construction of an extensive reaction network, guided by the abundance and reactivity of surface intermediates, yields transition-state-aware Brønsted–Evans–Polanyi relationships, which show improved predictive accuracy and can be generalized to longer-chain products. Within this framework, we provide the first mechanistic explanation of why Cu intrinsically disfavors low-value methane formation in favor of low-barrier C–C coupling steps, which directs the process toward higher-value oxygenates. By linking these mechanistic insights to design principles for Cu-centered multicomponent catalysts, our study supports the development of economically viable CO_2 conversion processes.

Introduction

Balancing environmental protection with industrial and technological growth has become a key global challenge.[1,2] Capturing and utilizing greenhouse gases,[3,4] particularly converting CO_2 into valuable C_{2+} chemicals *via* hydrogenation, has attracted substantial attention.[5] Most catalysts for these reactions contain Cu, which is known for high selectivity in CO_2 hydrogenation and, in particular, low yield of low-value HCOOH and CH_4 products.[6–11] Despite this recognition of Cu as a key catalyst component, a mechanistic explanation for its unique role remains elusive.

In this work, we provide an explanation for the uniqueness of Cu by addressing the complexity of the catalytic reaction network for CO_2 hydrogenation[12] into C_{2+} oxygenates, which significantly exceeds the notorious complexity of the CO hydrogenation reaction.[13–15] In particular, we discuss in detail the pathways of formation of key experimentally observed intermediates, including CO*, CHO*, HCOO*, COOH*, and CH_x*.[16–20]

Department of Chemical and Biomolecular Engineering, National University of Singapore, 4 Engineering Drive 4, Singapore 117585, Singapore.
E-mail: sergey.kozlov@nus.edu.sg

Although the modeling of catalytic reaction networks is incredibly helpful for understanding key factors driving various chemical reactions, the construction and analysis of microkinetic models covering reaction networks for CO_2 and CO hydrogenation is greatly complicated by the hundreds of involved intermediates.[13,15,21–25] In particular, the complexity of these models serves as the bottleneck for the rational design of new catalysts[26–29] through identifying key elementary steps and constructing Sabatier volcano plots.[30–32] Moreover, realistic modeling of chemical processes needs to account for the nanostructure of the applied catalysts[33,34] to minimize the gap between the computational predictions and the experimental observations. Indeed, nanostructuring is well-known for generating uniquely active sites with coordinatively unsaturated metal atoms on the catalyst surface.[35–37] Moreover, surface intermediates may diffuse between active sites under the high temperatures typical of heterogeneous catalytic hydrogenation.[38–40] Thus, advancing beyond simplistic models of ideal surfaces to more nuanced representations is essential for accurate simulations of complex, multistep catalytic processes.

Indeed, while numerous experimental studies focus on CO_2 hydrogenation into C_{2+} products on Cu, they typically omit mechanistic details explaining the aforementioned uniqueness of Cu. Experimental evidence of the activity of Cu-containing catalysts exists, for example, for K/Cu–Zn,[6] Cu–Pd,[7] Cu–CoO_x,[9] and Cu–Fe-based[10,11] systems, but lacks comprehensive mechanistic explanations, which require an extensive consideration of the reaction network. Some studies suggest that CO_2 hydrogenation to ethanol first involves the synthesis of methanol, which later decomposes into CH_3 species prone to C–C coupling, leading to the production of C_2 species such as ethanol.[8] While the vast majority of experimental studies investigated nanostructured catalysts (see references in a dedicated review[12]), previous theoretical studies either considered sub-nanoscale catalytic centers,[41] or focused on the idealized Cu(111) surfaces,[42] neglecting important active sites like nanoparticle edges, known to have key catalytic roles,[43] while omitting detailed mechanistic discussions. However, the urgent industrial need for highly selective CO_2 hydrogenation catalysts[44] calls for a more comprehensive mechanistic understanding of this reaction on catalyst models with a more realistic nanostructure.[45,46]

The mechanistic complexity of CO_2 hydrogenation toward C_{2+} oxygenates motivates systematic reaction network exploration, along with its rational reduction. Recently developed automated frameworks have demonstrated how large networks for heterogeneous catalysis can be generated on idealized models (typically single-crystal facets with a single site type).[47,48] For example, recent mechanistic studies on Cu have reported large sets of explicit transition states for CO_2 and CO hydrogenation and then used microkinetic simulations based on these transition states to compare competing routes and determine which pathways dominate.[49] However, further improvements in the realism of the employed models require accounting for nanostructuring effects and surface heterogeneity. Indeed, the very notion of a single, well-defined active site can be inappropriate under catalytic conditions, since structurally distinct active sites often coexist,[50,51] while reaction progress can require migration of intermediates from one site to another, see, *e.g.*, ref. 52. In turn, the applicability of BEP relationships may be limited in this context,[53] thus limiting the extent to which mechanistic models can be reduced using BEP relationships alone.

In order to address these challenges, we introduce an innovative approach that abstracts from the concept of a well-defined active site and accounts for the diffusion of reaction intermediates among diverse active sites exposed on the nanoparticle (NP) catalyst surface. Moreover, we propose a new ansatz to rationally simplify the catalytic network of such complex processes by selecting the most catalytically relevant bimolecular elementary steps involved in the reaction mechanism. As a result, the developed approaches allow us to obtain deeper insight into the CO_2 hydrogenation mechanism into C_2 compounds and extrapolate our results to the formation of C_{3+} products. In this study, we focus on Cu-based nanocatalysts due to their widespread use in both electro- and thermocatalytic CO_2 hydrogenation,[54–56] as well as a major component in multimetallic catalysts alongside metals like Co and Fe.[57–61] Moreover, we extend our analysis to CO_2 hydrogenation on Pd nanoparticles, which are commonly used for the hydrogenation of other compounds because of their very distinct electronic structure from Cu.[62] In addition, CuPd nanoparticles were proposed as an efficient catalyst for selective ethanol synthesis *via* CO_2 hydrogenation.[7]

Results and discussion

Structure of the active site

We go beyond the concept of discrete reactive sites on metal surfaces (top, bridge, or hollow) by accounting for the possibility of diffusion of surface intermediates within the (111) facet and its edges on nanoparticles, both of which are crucial for specific steps within the reaction network. Moreover, discrete sites such as hollow, bridge, or atop cannot support the growth of expanding C_n oxygenates/hydrocarbons of increasing size. Therefore, the reacting area in the model nanoparticle is expanded to the integrated active site shown in Fig. 1a. Below, we show that rapid surface diffusion of reaction intermediates can be assumed for Cu and, to a lesser extent, Pd. Hence, in our study, reactive species are considered to move freely across facets, potentially attaching to edge atoms as needed.

This integrated active site model is particularly well-suited to represent the local atomic environment of transition states in elementary steps. On fcc metals, a step or kink is essentially a concatenation of (111)/(100) edge atoms with coordination environments identical to the edge or corner sites modeled here. Therefore, a wide variety of active sites present on real nanoparticles is inherently captured within such a nanoparticle-based model.

To build a tractable catalytic reaction network including C_2 intermediates (with possible extension to C_{3+} intermediates), we introduce an ansatz where highly reactive surface adsorbates

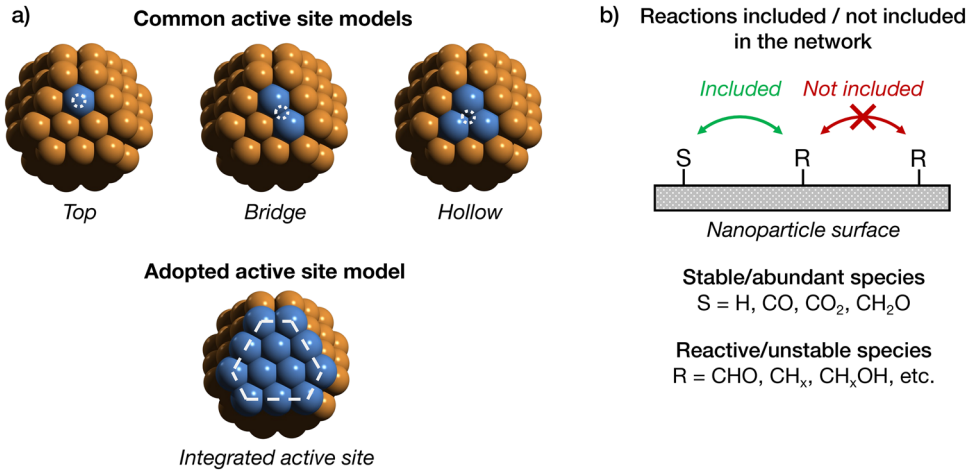

Fig. 1 Active site modeling and reaction network design approach. (a) Commonly employed discrete active site models *vs.* the adopted integrated active site model encompassing the entire (111) facet of the employed 1.1 nm large Cu_{79} nanoparticle model, including its edge atoms (dashed hexagon); (b) criterion for preselection of elementary steps in the reaction network based on occurrence and stability of intermediates.

preferentially interact with either relatively stable species (CO, CO_2, CH_2O) or species at high surface concentrations, like H* under high H_2 pressure,[63] as illustrated in Fig. 1b. That is, we assume that low concentrations of highly reactive or unstable species make reactions between them improbable. Such an approach is supported by most previous mechanistic studies, which proposed C–C bonds to form through coupling between highly reactive CH_x* (x = 1–3) species and CO or CO_2 on various catalysts.[7,44,64–67] In addition, we considered potential C–C coupling involving CH_2O intermediate due to its moderate stability in the gas phase, well-known high chemical reactivity, and possible involvement in the electrochemical CO_2 reduction mechanism.[19,20]

Focusing on abundant surface intermediates is consistent with microkinetic modeling, since these species dominate surface coverages (as discussed in Section S1, SI) and, therefore, make the most notable contributions to the overall reaction rates. Consequently, our ansatz is aimed at maintaining representability of the resulting network for subsequent microkinetic modeling without the excessive computational workload of exhaustive sampling of elementary steps. The outcome of elementary step preselection is shown in Section S1 of the SI, while the full reaction graph detailing activation barriers and free energies is covered in the following subsection. The original multistep methodology to explore extensive catalytic reaction networks is described in Section S2 of the SI.

Catalytic reaction network

The catalytic reaction network for the Cu catalyst is depicted as a directed graph in Fig. 2 (CO_2 hydrogenation on the Pd catalyst is discussed in Section S3 of the SI). Notably, the CO_2 hydrogenation network encompasses the CO hydrogenation network. The size of node circles indicates free energies at standard conditions relative to isolated CO_2^{gas} and H_2^{gas} (ΔG_n), considering that each C–O cleavage leading to the formation of OH* is then followed by the removal of H_2O from the surface. Edge colors in Fig. 2a represent elementary step barriers ($\Delta G^{\ddagger}$) calculated relative to their reference initial states. Fig. 2b summarizes the key steps and pathways discussed below. Note that $\Delta G^{\ddagger}$ includes the energy of co-adsorption of the reacting species, as detailed in Section S4 of the SI. While the Supplementary Spreadsheet file and Section S5 of the SI present a comprehensive tabulation of thermodynamic and kinetic parameters, we outline general reactivity trends below.

The graphs begin with CO_2 activation through formate and reverse water–gas shift pathways, charting C_1 and C_2 product formation *via* intermediates grouped into clusters encompassing methanediol, methanal, methanol, acetic acid, and others. CO_2 activation on Cu preferentially occurs *via* the formate pathway ($\Delta G^{\ddagger}$ = 0.71 eV), in line with previous experimental evidence on CO_2 hydrogenation using Cu-based catalysts,[68–70] followed by less kinetically favorable protonation of carboxylic oxygen to form HCOOH* ($\Delta G^{\ddagger}$ = 1.07 eV; see Section 2.4 for reaction nomenclature) and hydrogenation of the carboxylic carbon in HCOOH* ($\Delta G^{\ddagger}$[HCOOH* → OCH_2OH*] = 0.71 eV). The resultant OCH_2OH* readily releases OH* ($\Delta G^{\ddagger}$ = 0.24 eV) with the formation of formaldehyde, which easily desorbs (ΔG = −0.01 eV at 1 bar and 273.15 K). Since the barrier of OCH_2OH* transformation into CH_2O* is low, this intermediate is unlikely to accumulate and be observed experimentally. Further hydrogenation of CH_2O* into CH_3O* upon readsorption is also feasible ($\Delta G^{\ddagger}$ = 0.39 eV). In line with the relative stability of the latter under *operando* conditions during CO_2 hydrogenation over Cu-based catalysts,[16,71] the predicted protonation barrier for CH_3O* is relatively high, 1.18 eV, after which CH_3OH easily desorbs, serving as the endpoint for CO_2 hydrogenation on pristine Cu.

The transition from CH_xOH* to CH_x* (x = 1–3) intermediates requires overcoming significant energy barriers, which hinder the transition between C_1 and C_2 species in the reaction network (see full data in the supplementary spreadsheet). Due to high barriers for CH_x formation through C–O cleavage,

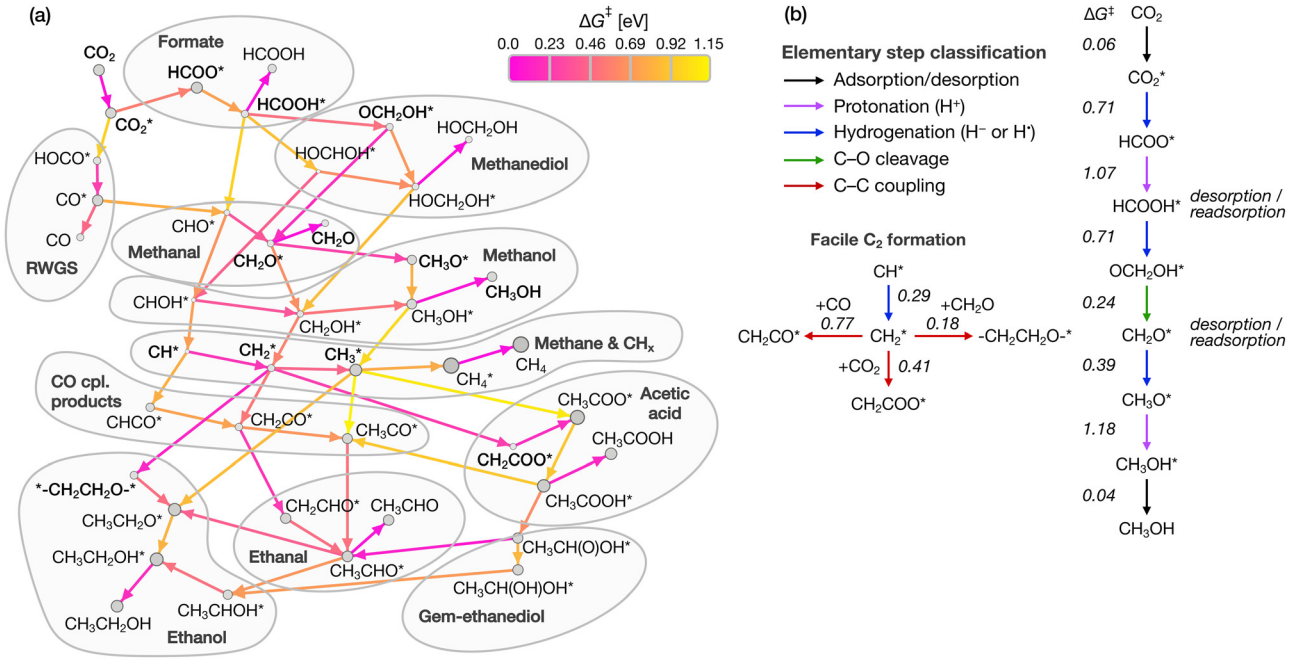

Fig. 2 Catalytic reaction network on Cu. (a) Directed graph with elementary step barriers calculated relative to the respective initial states, $\Delta G^{\ddagger}$, encoded in edges. The size of the node circles reflects relative stability, measured by ΔG_n, where the largest nodes indicate the highest stability and *vice versa*. Key intermediates are marked with semi-bold typeface. (b) Key elementary steps and intermediates in C_1 and C_2 transformations discussed in the text, as well as the classification of elementary steps.

methanol remains the predominant product in CO_2 hydrogenation on pristine Cu nanoparticles. Indeed, the formation of methanol catalyzed by Cu-based systems is well-known (*e.g.*, see ref. 16 and 71), and previous theoretical studies of methanol formation on Cu reported very similar reaction pathways.[72,73]

At the same time, Cu(111) facets show advantageous catalytic activity in transformations of the CH_x species. Within the CH_x cluster, hydrogenation barriers increase progressively from CH* to CH_3* ($\Delta G^{\ddagger}$ = 0.29, 0.63, and 1.15 eV for CH* → CH_2*, CH_2* → CH_3*, and CH_3* → CH_4*), which indicates poor catalytic activity of Cu in the synthesis of low-value methane as a product. More importantly, CH_2* hydrogenation is less favorable than two out of three concurrent C–C coupling reactions between CH_2* and various species in the reaction environment:

$$CH_2^* + CH_2O^* \rightarrow -CH_2CH_2O-^* \quad (\Delta G^{\ddagger} = 0.18\ \text{eV}),$$

$$CH_2^* + CO^* \rightarrow CH_2CO^* \quad (\Delta G^{\ddagger} = 0.77\ \text{eV}),$$

$$CH_2^* + CO_2 \rightarrow CH_2COO^* \quad (\Delta G^{\ddagger} = 0.41\ \text{eV}).$$

Thus, the final C_2 oxygenate clusters can be formed on Cu *via* two kinetically feasible pathways. First, CH_2* can couple with CH_2O to form $-CH_2CH_2O-$*, which is an intermediate in ethanol synthesis. This elementary step has not been previously reported for thermocatalytic CO_2 hydrogenation on metallic Cu and is therefore proposed here as a new mechanistic route. However, similar coupling reactions involving CH_2O have been observed on Cu in electrocatalytic CO_2/CO reduction, where *CHO–CH_2O and *CO–CH_2O coupling steps appear in ethanol formation pathways.[19,20] This CH_2O-driven pathway to C_2 products is plausible because CH_2O* desorption is kinetically preferred to its hydrogenation to CH_3OH, enabling gas-phase methanal to re-adsorb and couple with other species. Prior studies have also noted the scarcity of CH_2O signatures in operando spectra of Cu-based catalysts, which supports its fast turnover or desorption.[72]

Second, the facile coupling between CH_2* and CO_2, leading to CH_2COO*, aligns with recent observations of carboxylic acid formation in CO_2 hydrogenation on Fe–Zn, Ni–Zn, and Co–Mn catalysts.[74–76] To the best of our knowledge, this CH_2–CO_2 coupling route on metallic Cu has not been reported previously, and is thus introduced here as a new thermocatalytic mechanism to Cu. A related product distribution, including acetic acid and ethanol, has also been observed on non-metallic Cu-zeolite catalysts, which rely on distinct confined sites.[77]

Thus, despite the high kinetic barrier for the formation of CH_x species on Cu, they are calculated to readily react with either CO_2, CO, or H_2CO species in the reaction environment to form the desirable C_2 products. As a result, Cu is frequently used as one of the components in multimetallic catalysts together with metals like Co, which can easily form CH_x species on the pathway of complete CO_2 hydrogenation into methane.[78,79] The combination of Cu with other metals could allow the catalyst to bypass the high-energy barriers between methanol and CH_x intermediate clusters with the help of the

co-catalyst and enable the subsequent C–C steps involving CH_x intermediates on Cu sites.

Surface diffusion of intermediates and catalytic activity of nanoparticle edges

In this section, we discuss the surface diffusion of chemisorbed intermediates, assuming that valence-saturated parts of alkyl chains can only physisorb on the surface due to dispersion attraction. Since dispersion interactions are quite weak for rather small C_1 and C_2 species and vary very smoothly with the atomic positions, they are known to have a minor effect on diffusion barriers.[80] For example, the adsorption free energy of CH_4 on Cu(111) and Pd(111) is 0.03 and ∼0.00 eV, respectively, indicating that the enthalpy of physisorption has roughly the same magnitude as the free energy contribution of the entropic stabilization of the gas phase molecules.

For this analysis, we chose CH*, CH_2*, and CH_3* as model intermediates to investigate the diffusion of adsorbed RC* (sp carbon), RHC* (sp^2 carbon), and RH_2C* (sp^3 carbon) groups (R = alkyl), capturing the primary carbon binding modes to the metal surface. In turn, OH* was selected to model RO* surface species.

The weakly binding Cu(111) surface facilitates easy migration of adsorbates chemisorbed through sp, sp^2, and sp^3 carbon centers or O atoms, as shown in Fig. 3a–c. Notably, all diffusion barriers (red in Fig. 3a–d) are significantly lower than those of the reaction steps involving CH_x species in the catalytic network. This includes OH* and CO* migration involved in the forward and reverse C–O cleavage and the coupling of CO* molecules with other reaction intermediates. This indicates that surface diffusion within the facets and edges of Cu NPs is much faster than most of the elementary steps of the considered catalytic process.

Two critical steps in the reaction network occur exclusively or preferentially on edges between (111) facets. The first is CO_2 hydrogenation into HCOO* or HOCO* *via* formate or RWGS pathways (Fig. 2), whereas for HCOO* formation on Cu, we were able to locate TS both on the facets ($\Delta G^{\ddagger}$ = 0.82 eV) and the edges ($\Delta G^{\ddagger}$ = 0.71 eV), and the obtained transition states for all other CO_2 activation steps necessarily involved NP edge atoms. The second step involving edge atoms in TS is facile C–O cleavage in methanediolate OCH_2OH* intermediate to produce CH_2O ($\Delta G^{\ddagger}$ = 0.24 eV), which is a crucial step for the subsequent hydrogenation reactions on Cu. Other less significant reaction steps may also occur at or near edge sites, as detailed in the supplementary spreadsheet.

Note that the facile surface diffusion of most intermediate species does not imply the negligible effect of the distinction

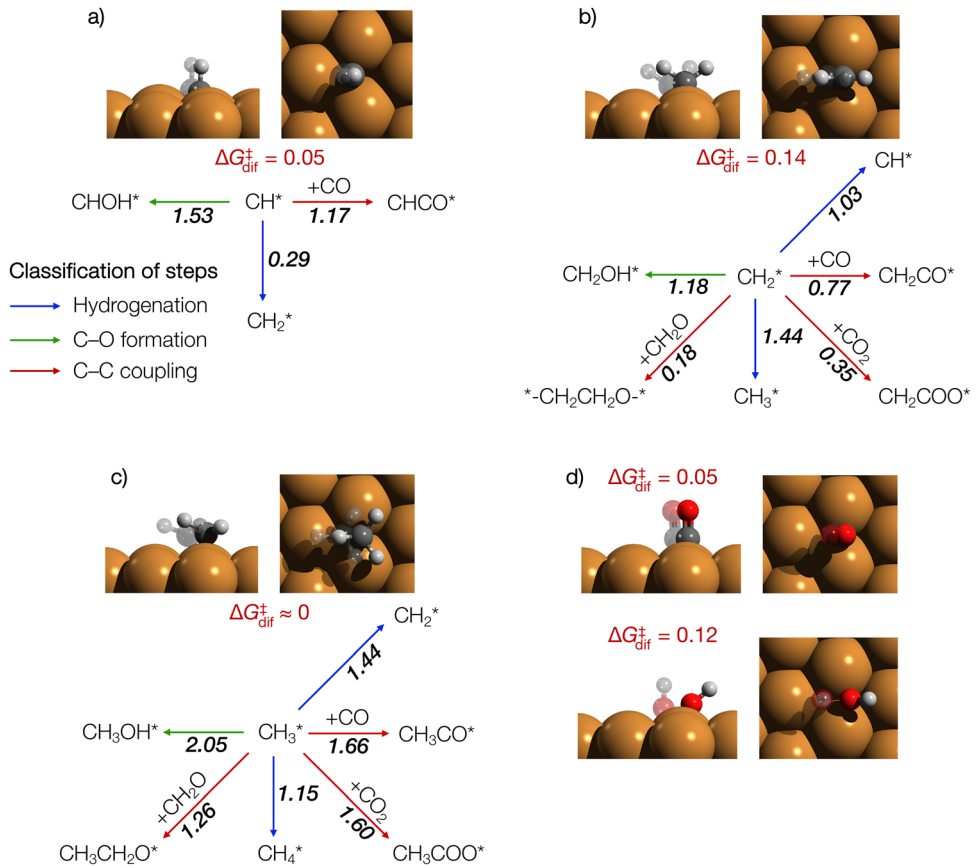

Fig. 3 Diffusion transition states (opaque) and minima on the PES (translucent) on the (111) facet of a Cu nanoparticle. Intermediates considered: (a) CH*; (b) CH_2*; (c) CH_3*; (d) CO* and OH*. Only the relevant areas on the NP are shown. Diffusion barriers $\Delta G^{\ddagger}$ are shown in red, alongside the barriers for elementary steps involving the respective species in the reaction network; Cu is represented in dark orange, O in red, C in dark grey, and H in light grey. All values are in eV.

between catalytic activities of edge and terrace sites on the reaction kinetics. Indeed, edges and other low-coordination sites are far less common than (111) facets on the catalyst surface, and their surface concentration diminishes as the catalyst nanoparticle size grows. Consequently, key reaction steps at these sparse sites could become a bottleneck for catalytic activity, unless addressed in catalyst design.

BEP relationships and reactivity trends

We analyzed the trends in the considered elementary steps using the Brønsted–Evans–Polanyi (BEP) principle, which states that, for a given elementary step within a family of similar reactions, the activation energy linearly correlates with the reaction energy.[81] Strictly speaking, the BEP principle implies that transition states for the examined elementary step should be structurally similar on the considered catalysts. However, this condition is rarely examined during the construction and application of BEP relationships (see a rare example in ref. 82). Previous approaches to formulating BEP relationships typically relied on separating reactions by bond or reaction type (*e.g.*, hydrogenation *vs.* C–C coupling *vs.* C–O cleavage).[83–85] In contrast, we show below that focusing solely on the chemical bond or reaction type can be insufficient, as bonds such as C–C or C–O may form *via* distinct transition states (equivalent to distinct mechanisms) that require separate BEP relationships. Similarly, even hydrogenation and protonation reactions may proceed *via* structurally different transition states and follow several distinct BEP relationships.

In this study, we applied the concept of TS structural similarity to clustering reaction steps on either Cu or Pd, revealing more accurate correlations between activation and reaction energies (Fig. 4; see Section S2 for details of the linear fitting procedure). For hydrogenation steps (Fig. 4a), we identify two TS types where, formally, $H^{\bullet}$ or H^{-} bind to surface intermediates (see the charge analysis in Section S6). The pink data points in Fig. 4 correspond to hydrogen associating with carbon in a tetrahedral sp^3-like TS, leading to sp^3 products in hydrogenations of **C**H_3*, **C**H_2COOH*, CH_3**C**HOH*, *etc.* (here and below, the reacting atom is given in bold). Some seemingly sp^2 centers like CH_2* lie within this BEP due to the tetrahedral TS in which the intermediate binds to two metal atoms in sp^3-like geometry. The linear regression of activation and reaction energies for these steps yields low RMSD values of 0.12 eV for Cu and 0.06 eV for Pd, which is well below DFT accuracy benchmarks.[86] Notably, CH_3* hydrogenation on Cu is an outlier ($\Delta G^{\ddagger}$ = 1.15 eV, Fig. 4a, left), possibly because CH_3* partially detaches from the nanoparticle in TS, leading to physisorbed CH_4, unlike in other steps where the products remain surface-bound.

Another hydrogenation type involves, formally, $H^{\bullet}$ or H^{-} reacting with sp^2 centers (violet data in Fig. 4a). The TS structures in these elementary steps resemble those in the Felkin–Anh model for nucleophilic addition to carbonyls,[87] here seen in the hydrogenation of carbonyl-bearing species like **C**H_2O*, **C**HO*, and CH_3**C**HO*. Some non-carbonyl CH_2 centers in **C**H_2CO and **C**H_2CHO*, as well as sp^2 geometries in bridge CO*, **C**(H)OH, and bridge **C**H*, also fit this BEP relationship due to similar geometries. Linear fits show remarkably low RMSD values of 0.10 eV for Cu and 0.09 eV for Pd.

This approach to the analysis of BEP relationships diverges from previous studies[31,84,88] that assigned a single BEP to reaction types like hydrogenation, C–O cleavage, or C–C coupling, ignoring variations in the TS geometry. However, tailoring BEP relationships to transition state structures has notably increased the correlation quality. For example, including both sp^2 and sp^3-like transition states into the BEP relationship for the hydrogenation steps increases its RMSD to 0.22 eV from 0.10 and 0.12 eV obtained in Fig. 4a. Similarly, clustering of calculated data points according to the TS geometry consistently improves the quality of BEP relationships for all types of elementary steps.

Note that the hydrogenation steps considered above did not include protonation steps, where surface H species attach to O atoms in the CO_2 hydrogenation intermediates (Fig. 4b). One can notice the abnormally negative slope in BEP relationships for protonation on Cu catalysts, which is rationalized in Section S4 by careful analysis of co-adsorption effects. The considered protonation elementary steps can also be classified into two groups.

In the first group, the protonation elementary steps involve the hydroxyl group's acid–base chemistry (blue in Fig. 4b), encompassing alcoholate species like **O**H*, CH_3**O***, **O**CH_2OH*, and carbonyl oxygen protonation in, *e.g.*, CH**O***, CH_2**O***, CH_3CH**O***. The structure of TS for these elementary steps resembles the product bearing an OH group, akin to the late transition state within the framework of Hammond's postulate. Fig. S9 in Section S7 illustrates these late TS, where the alpha-carbon binds to the metal, forming an alcoholate that abstracts H from the catalyst surface. Linear BEP relationships for these reaction steps on Cu and Pd yield an RMSD of 0.08 eV. Notable outliers include the facile protonation of CH_2**O*** on Cu with $\Delta G^{\ddagger}$ = 0.93 eV and ΔG = −0.25 eV and the kinetically hampered protonation of CH_3CH_2**O*** on Pd with $\Delta G^{\ddagger}$ = 0.84 eV (likely due to the unusual coordination of two Pd atoms by O, see Fig. S9). The high barrier for OH* protonation on Cu ($\Delta G^{\ddagger}$ = 1.35 eV, Fig. 4b, left) highlights the need for promoters or co-catalysts to avoid OH poisoning of this catalyst and facilitate the regeneration of the active sites *via* water formation and desorption.

Another BEP relationship is followed by the protonation steps involving the carboxyl group (green data in Fig. 4b). On Cu, the carboxyl group of HCOOH* keeps its characteristic planar geometry in the TS during the transformation:

$$\mathrm{HCOOH^* + H^* \rightarrow HOCHOH^*},$$

whereas on Pd, HCOOH* adopts a non-planar configuration (Fig. S10). Hence, HCOOH* protonation on Pd is categorized under the RO^- family of elementary steps for alcoholates, whereas on Cu, it is attributed to the $RCOO^-$ protonation family. Linear fits reveal significant intercept differences, showing easier RO^- protonations on Cu and easier $RCOO^-$ protonation on Pd. Note that due to limited data points, the obtained BEP correlations, in this case, are more suitable for classifying

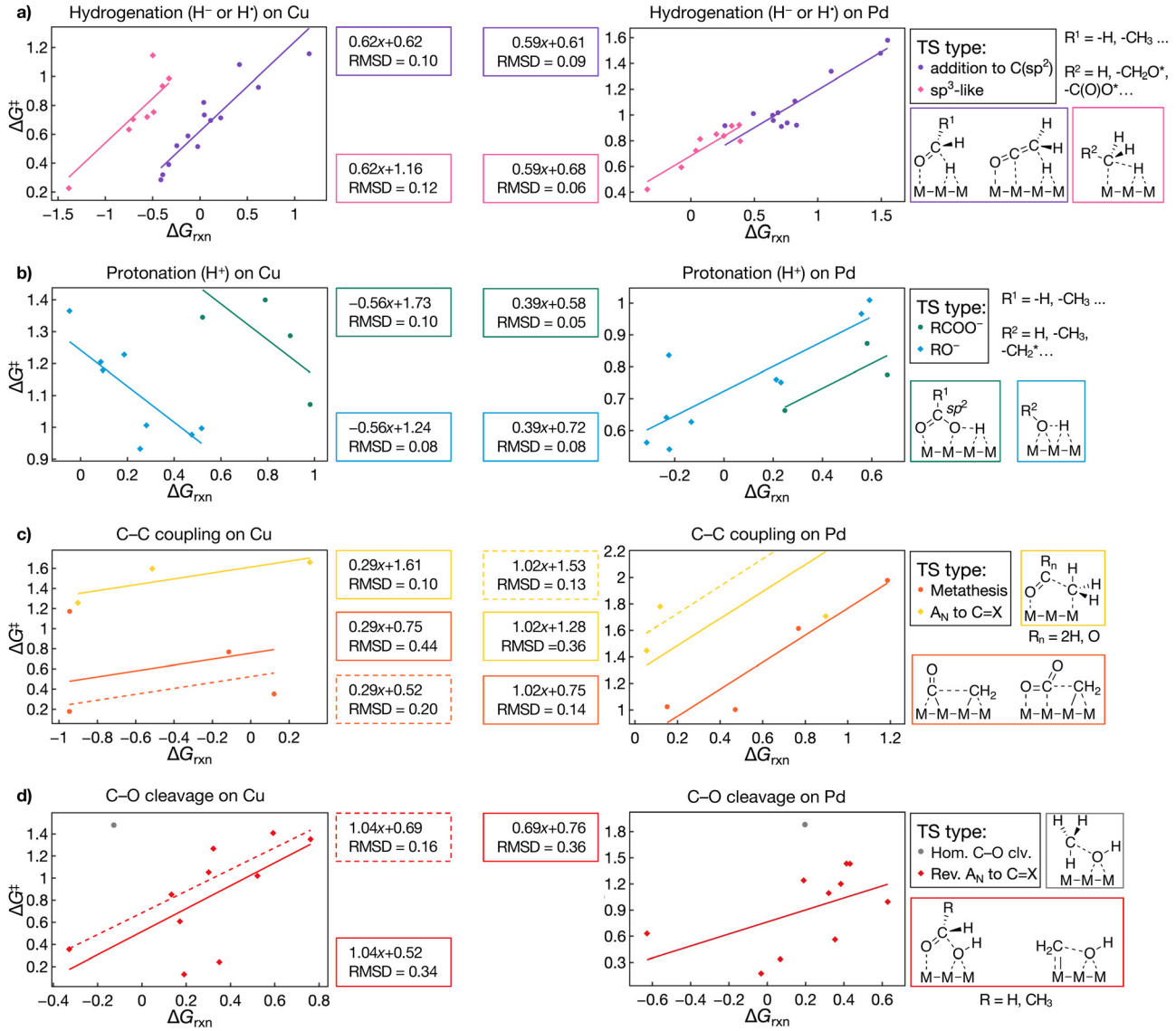

Fig. 4 BEP relationships (in eV) for different classes of elementary steps on Cu (left) and Pd (right) catalysts. Steps considered: (a) hydrogenation; (b) protonation; (c) C–C coupling; (d) C–O cleavage steps. Typical transition state structures are illustrated on the right side of the figure, with forming and breaking bonds indicated by dashed lines. The yellow dashed line in Fig. 4c (right) was extrapolated for clarity.

reaction steps rather than numerical estimates of activation energies, although they still yield low RMSD values of 0.10 for Cu and 0.05 for Pd.

The next reaction class, C–C coupling, also shows two TS types differentiated by reactant structures. Couplings of formally nucleophilic $CH_3^{\bullet}$:

$$CH_3^* + CH_2O^* \rightarrow CH_3CH_2O^*,$$

$$CH_3^* + CO_2^* \rightarrow CH_3COO^*,$$

$$CH_3^* + CO^* \rightarrow CH_3CO^*$$

occur *via* a TS akin to nucleophilic addition to carbonyls, where CH_3 migrates from the metal to the carbon (yellow data in Fig. 4c). Fewer data points were calculated for this family of elementary steps than for more abundant hydrogenation or protonation steps in the reaction network. The three data points calculated for Cu follow the same BEP relationship with an RMSD of 0.10 eV. At the same time, the correlation between the reaction and activation energies of these steps is less clear on Pd catalysts. In this case, the CH_3* and CO* association is an outlier from the obtained BEP relationship, raising its RMSD to 0.36 eV (solid line in Fig. 4c; see the structure in Fig. S11) from 0.13 without it (dashed line).

Another type of C–C coupling involves intermediates with double or triple bonds, such as CO_2* and CO*, as well as bridge-bonded CH_x* (x = 1–2). In these cases, the bond multiplicity in the CO- or CO_2-containing moiety decreases, while the CH_x moiety becomes singly bonded to the surface, leading to the formation of a new C–C bond. Due to this bond redistribution,

this class is designated as metathesis (dark orange data in Fig. 4c). Linear regression of all data points calculated on Pd catalysts yields an RMSD of 0.14 eV. On Cu, the BEP relationship for all such steps has an RMSD of 0.44 eV (solid orange line in Fig. 4c), which decreases to 0.20 eV if one outlier, CH* coupling with CO*, is removed from the analysis (dashed orange line in Fig. 4c; see the structure in Fig. S11). Such deviation of CH*–CO* coupling from the common trend indicates that the transition state for this reaction on Cu may need to be attributed to another TS class, which has not been comprehensively represented in the considered reaction network.

The final reaction class involves C–O cleavage, featuring a predominant TS type akin to the reverse of OH^- nucleophilic addition to carbonyls (red data in Fig. 4d). Both cleavage products, OH* and the organic moiety, remain bound to the metal surface in the transition and final states. Significant outliers from BEP relationships on both Cu and Pd catalysts (structures in Fig. S12) include:

$$OCH_2OH^* \rightarrow CH_2O^* + OH^*$$
$$(\Delta G^{\ddagger} = 0.24 \text{ eV on Cu, } 0.34 \text{ eV on Pd}),$$

$$CH_3CH(O)OH^* \rightarrow CH_3CHO^* + OH^*$$
$$(\Delta G^{\ddagger} = 0.13 \text{ eV on Cu, } 0.18 \text{ eV on Pd}).$$

Excluding these outliers from BEP correlation on Cu catalysts lowers its RMSD from 0.34 to 0.16 eV. The divergence of these elementary steps from BEP relationships likely results from the involvement of low-coordination edge sites in the TS and the aldehyde moiety bonding *via* O to the surface, unlike other C–O cleavages, where surface bonding occurs *via* C. We did not isolate these two elementary steps into a separate BEP due to their low number, although site-specific BEPs are generally recommended.[89]

Finally, CH_3OH features a unique C–O cleavage mechanism where the CH_3 group becomes unattached to the metal surface in the TS on both Cu and Pd catalysts (grey data point in Fig. 4d; structure in Fig. S13). Here, CH_3 adopts a planar configuration indicative of either the CH_3^+ or $CH_3^\bullet$ state (unlike strictly non-planar CH_3^-).[90] Bader charge analysis in Fig. S13 shows that the carbon atom of the CH_3 moiety in the TS bears a slightly negative charge, confirming the $CH_3^\bullet$ state. The imaginary vibrational mode in these TS shows $CH_3^\bullet$ moving into the gas phase, indicating that this cleavage in CH_3OH on both metals resembles a classic homolytic bond cleavage, yielding $CH_3^\bullet$ and OH*.

In general, our analysis reveals significant differences between BEP relationships calculated on Cu and Pd for various elementary steps. A discussion of BEP relationships within the presented catalytic reaction network, extended to a broader set of metals, is available elsewhere.[91] This finding strongly deviates from the widespread understanding of BEP relationships and their common application across various metals in computational catalyst design studies.[92,93] In particular, the derived BEP relationships highlight the exceptional catalytic properties of Cu discussed earlier. Cu is calculated to be generally more active than Pd in hydrogenation steps despite the well-recognized activity of the latter in hydrogenation catalysis. Moreover, the only step with an unusually high hydrogenation barrier on Cu catalysts is the hydrogenation of CH_3* to methane, which is considered an undesired product in most industrial processes. In turn, protonation barriers on Cu generally exceed 1 eV, contrasting with notably lower protonation barriers of Pd, which is in line with much more negative charge on H* atoms adsorbed on the former (Section S6). Moreover, copper's notable activity in C–C coupling *via* metathesis transition states (Fig. 4c) distinguishes it from Pd (Section S3). Both metals show a broad range of C–O cleavage barriers (0.2 to 1.5 eV) with low barriers only for the OH elimination from OCH_2OH* and $CH_3CH(O)OH$* catalyzed by NP edges, leading to the formation of CH_2O* and CH_3CHO* (see the equations above). These findings highlight that both Pd and Cu may need promoters or co-catalysts (*e.g.*, Co) to facilitate the other higher-barrier C–O cleavage steps. In particular, Cu catalysts have low activity in OH* protonation, which is necessary for the production of water byproduct and regeneration of active sites on the catalyst.

The differences between catalytic trends calculated on Cu and Pd suggest that mixed Cu–Pd catalysts may have improved activity in CO_2 hydrogenation. Indeed, Pd sites are highly active in CO_2 hydrogenation to CO (which poisons Pd at low temperatures) and in the conversion of the formed OH* into H_2O, necessary to close the cycle and return the catalyst to its initial state (see Section S3 for details). The produced CO* is very mobile on the catalyst surface and may migrate towards Cu sites *via* a desorption/readsorption mechanism. In turn, Cu catalysts are quite active in further selective hydrogenation of CO with minimal methane by-product formation as well as C–C coupling steps. Thus, our analysis is in line with recent experimental mechanistic studies of highly selective CO_2 hydrogenation to ethanol on Pd_2Cu catalysts, which identified CO* hydrogenation into HCO* as the rate-limiting step, alleviating the CO* poisoning of the catalyst.[7]

Summary and conclusions

We introduced a new methodology for constructing and disentangling catalytic reaction networks and applied it to the analysis of CO_2 conversion into value-added chemicals. Our methodology merges rapid semi-empirical explorations with accurate DFT modeling to understand diverse reaction pathways. It speeds up the identification of key intermediates and clarifies catalytic mechanisms, providing deep insights into catalytic behavior. Moreover, our study provides a more realistic representation of nanostructured catalysts, including facet and edge sites as well as facile diffusion of adsorbates between them, which is shown to be crucial for the understanding of CO_2 hydrogenation kinetics and rational design of catalysts for this reaction. The importance of considering both facets and edges in nanoparticle models cannot be overstated, as they

account for the diversity of active sites in real-world catalysts, thereby enhancing our understanding of catalytic behavior and aiding in the rational design of materials with optimized surface features.

Our catalytic network analysis reveals the ability of Cu to selectively produce methanol in CO_2 hydrogenation and suggests the promising potential of Cu-based catalysts for the synthesis of C_2 oxygenates with the help of co-catalysts in multicomponent systems. Notably, we highlight the role of formaldehyde as a functionally pivotal intermediate, leading either to methanol or, *via* coupling with CH_2*, to ethanol precursors. This branching point defines the unique reactivity of Cu: CH_2* can participate in multiple low-barrier C–C coupling steps, while further hydrogenation of CH_x species to methane is kinetically hindered. This relative inactivity of Cu in methanation reactions, coupled with facile C–C formation once CH_2* is accessed, defines a selectivity pattern in line with experimental studies. Moreover, the catalytic activity of Cu is further increased by the rapid surface diffusion of the reaction intermediates, which allows the facet and edge sites to function as an integrated active site.

These insights translate into a set of suggestions for the design of Cu-based catalysts. First, catalyst nanoparticles can be engineered with abundant or stabilized low-coordinated sites to facilitate steps requiring undercoordinated metal atoms (CO_2 activation; OCH_2OH* decomposition into CH_2O*). Second, high activity of Cu in C–C coupling steps can be exploited by mixing Cu with components such as dopants, CoO_x, or acidic supports bearing OH groups, to promote the identified high-barrier steps (protonation and C–O cleavage). Indeed, hydroxyl-rich oxide supports have been reported to enhance the selectivity of CO_2 hydrogenation to ethanol by stabilizing oxygenated intermediates and enabling subsequent C–C coupling processes on various catalysts.[8,64,94]

Moreover, we establish highly accurate transition-state-aware BEP relationships for critical elementary steps in CO_2 hydrogenation to facilitate further computational studies of this reaction. These BEP relationships apply to C_{3+} pathways that include iterative CH_2 insertions *via* similar transition states, like those involving C_{1-2} intermediates analyzed here. The obtained BEP relationships were found to be significantly different on Cu and Pd catalysts, suggesting the necessity to reevaluate the transferability of BEP relationships between various materials. This suggests that BEPs should be formulated only for reactions with similar transition state classes or adsorbate coordination motifs, which could change with metal catalyst identity or alloy composition. Otherwise, the predictive accuracy of the constructed BEP will degrade. Therefore, high-throughput screening studies in computational catalyst design should apply transition-state-class-specific BEPs, in accordance with representative site and binding motifs rather than relying on a single "universal" relationship. Since the structures of the pre-reaction intermediates are sufficient to determine the transition state class (as the reacting functional group dictates the TS structure), the proposed approach to the construction of accurate BEP relationships paves the way for machine learning applications in rational catalyst design.

This work is meant as a blueprint for future research in CO_2 hydrogenation, introducing methods for the rapid and precise exploration of reaction networks through advanced quantum chemical techniques. Although selective CO_2 hydrogenation to valuable chemicals is technically complex and challenging, this reaction offers an opportunity for sustainable and CO_2-negative chemical synthesis; our methodologies and insights are instrumental in addressing this complexity in the goal of designing catalysts for the carbon-neutral economy.

Methods

Since a new multistep methodology was employed in constructing the reaction network, a detailed description of the methodology, computational parameters, and the rationale for the choice of the DFT functional is provided in the SI, while the main methods are summarized here. Spin-polarized DFT calculations were performed using the revPBE[95] functional in VASP 6.3.2. We set a plane-wave energy cutoff at 415 eV and employed the PAW method.[96] Dispersion was accounted for *via* the DFT-D3 scheme with Becke–Johnson damping.[97,98] System geometries were pre-optimized using the GFN1-xTB method[99] in ASE[100] (see the SI for details on the multistep procedure for high-throughput semi-empirical reaction network exploration).

The reactivities of Cu and Pd catalysts were modelled using bare unsupported Cu_{79} and Pd_{79} to focus on the intrinsic reactivity of the metal sites, as mentioned above. Such unsupported nanoparticle models closely mimic the properties of nanoparticles supported on inert materials, such as MgO[101] and graphene,[102] whereas more active supports could have a stronger effect on the catalyst activity.[103] For example, our recent studies indicate that crystalline C_{60} or ZnO[102,104] can affect the barriers for electrochemical or thermal CO_2 reduction or hydrogenation barriers by up to 0.3 eV on highly active Pd and Cu catalysts, respectively.[103] The full description of the models is provided in the SI.

Author contributions

Mikhail V. Polynski: conceptualization; formal analysis; investigation; methodology; writing – original draft; writing – review & editing. Sergey M. Kozlov: conceptualization; resources; writing – review & editing.

Conflicts of interest

There are no conflicts to declare.

Data availability

The data underlying this study are available in the published article and its supplementary information (SI). Python code for fast reaction network exploration is available in the supplementary ZIP archive and in a dedicated GitHub repository.[105] A complete listing of computational details is available in the SI.

The supplementary spreadsheet includes all total electron energies, reaction Gibbs free energies, and free energies of activation. The supplementary ZIP archive includes all structures of intermediates and transition states in the XYZ format. Supplementary information is available. See DOI: https://doi.org/10.1039/d5ey00338e.

Acknowledgements

The authors gratefully acknowledge the financial support provided by the National Research Foundation Singapore, under its Campus for Research Excellence and Technological Enterprise (CREATE) programme (Development of Advanced Catalysts for Electrochemical Carbon Abatement, Project Code: 370184872) and by the Agency for Science, Technology and Research (A*Star) through the grant LCERFI01-0033|U2102 d2006. Computational work was performed using resources of the National Supercomputing Centre, Singapore.

References

1 E. Y. Zeng, J. You and H. Cheng, Balance between economic growth and environmental protection: sustainability through better science, *J. Environ. Monit.*, 2011, **13**, 787–788.
2 A. Shakoor and R. Ahmed, The environmental sustainable development goals and economic growth: an empirical investigation of selected SAARC countries, *Environ. Sci. Pollut. Res. Int.*, 2023, **30**, 116018–116038.
3 W. Gao, S. Liang, R. Wang, Q. Jiang, Y. Zhang, Q. Zheng, B. Xie, C. Y. Toe, X. Zhu, J. Wang, L. Huang, Y. Gao, Z. Wang, C. Jo, Q. Wang, L. Wang, Y. Liu, B. Louis, J. Scott, A. C. Roger, R. Amal, H. He and S. E. Park, Industrial carbon dioxide capture and utilization: state of the art and future challenges, *Chem. Soc. Rev.*, 2020, **49**, 8584–8686.
4 S. Sun, H. Sun, P. T. Williams and C. Wu, Recent advances in integrated CO_2 capture and utilization: a review, *Sustainable Energy Fuels*, 2021, **5**, 4546–4559.
5 G. Prieto, Carbon Dioxide Hydrogenation into Higher Hydrocarbons and Oxygenates: Thermodynamic and Kinetic Bounds and Progress with Heterogeneous and Homogeneous Catalysis, *ChemSusChem*, 2017, **10**, 1056–1070.
6 H. Guo, S. Li, F. Peng, H. Zhang, L. Xiong, C. Huang, C. Wang and X. Chen, Roles Investigation of Promoters in K/Cu–Zn Catalyst and Higher Alcohols Synthesis from CO_2 Hydrogenation over a Novel Two-Stage Bed Catalyst Combination System, *Catal. Lett.*, 2015, **145**, 620–630.
7 S. Bai, Q. Shao, P. Wang, Q. Dai, X. Wang and X. Huang, Highly Active and Selective Hydrogenation of CO_2 to Ethanol by Ordered Pd–Cu Nanoparticles, *J. Am. Chem. Soc.*, 2017, **139**, 6827–6830.
8 L. Ding, T. Shi, J. Gu, Y. Cui, Z. Zhang, C. Yang, T. Chen, M. Lin, P. Wang, N. Xue, L. Peng, X. Guo, Y. Zhu, Z. Chen and W. Ding, CO_2 Hydrogenation to Ethanol over Cu@Na-Beta, *Chem*, 2020, **6**, 2673–2689.
9 Y. Zhang, G. Fan, L. Zheng and F. Li, Synergistic Surface-Interface Catalysis in Potassium-Loaded Cu/CoO_x Catalysts to Boost Ethanol Production from CO_2 Hydrogenation, *ACS Appl. Mater. Interfaces*, 2025, **17**(9), 13747–13761.
10 D. Xu, M. Ding, X. Hong and G. Liu, Mechanistic aspects of the role of K promotion on Cu–Fe-based catalysts for higher alcohol synthesis from CO_2 hydrogenation, *ACS Catal.*, 2020, **10**, 14516–14526.
11 D. Xu, M. Ding, X. Hong, G. Liu and S. C. E. Tsang, Selective C^{2+} Alcohol Synthesis from Direct CO_2 Hydrogenation over a Cs-Promoted Cu–Fe–Zn Catalyst, *ACS Catal.*, 2020, **10**, 5250–5260.
12 Y. Sheng, M. V. Polynski, M. K. Eswaran, B. Zhang, A. M. H. Lim, L. Zhang, J. Jiang, W. Liu and S. M. Kozlov, A review of mechanistic insights into CO_2 reduction to higher alcohols for rational catalyst design, *Appl. Catal., B*, 2024, **343**, 123550.
13 Z. W. Ulissi, A. J. Medford, T. Bligaard and J. K. Nørskov, To address surface reaction network complexity using scaling relations machine learning and DFT calculations, *Nat. Commun.*, 2017, **8**, 14621.
14 A. Cao, J. Schumann, T. Wang, L. Zhang, J. Xiao, P. Bothra, Y. Liu, F. Abild-Pedersen and J. K. Nørskov, Mechanistic Insights into the Synthesis of Higher Alcohols from Syngas on CuCo Alloys, *ACS Catal.*, 2018, **8**, 10148–10155.
15 J. Schumann, A. J. Medford, J. S. Yoo, Z. J. Zhao, P. Bothra, A. Cao, F. Studt, F. Abild-Pedersen and J. K. Nørskov, Selectivity of Synthesis Gas Conversion to C^{2+} Oxygenates on fcc(111) Transition-Metal Surfaces, *ACS Catal.*, 2018, **8**, 3447–3453.
16 Q. Sun, C. W. Liu, W. Pan, Q. M. Zhu and J. F. Deng, In situ IR studies on the mechanism of methanol synthesis over an ultrafine Cu/ZnO/Al_2O_3 catalyst, *Appl. Catal., A*, 1998, **171**, 301–308.
17 T. T. Mamo, M. Qorbani, A. G. Hailemariam, R. Putikam, C. M. Chu, T. R. Ko, A. Sabbah, C. Y. Huang, S. Kholimatussadiah, T. Billo, M. K. Hussien, S. Y. Chang, M. C. Lin, W. Y. Woon, H. L. Wu, K. T. Wong, L. C. Chen and K. H. Chen, Enhanced CO_2 photoreduction to CH_4 via *COOH and *CHO intermediates stabilization by synergistic effect of implanted P and S vacancy in thin-film SnS_2, *Nano Energy*, 2024, **128**, 109863.
18 Z. Gao, G. Gao, C. Li, H. Tian, Q. Xu, S. Zhang, L. Xu and X. Hu, Interaction of the reaction intermediates in co-reforming of acetic acid and ethanol impacts coke properties, *Mol. Catal.*, 2021, **504**, 111461.
19 A. Herzog, A. Bergmann, H. S. Jeon, J. Timoshenko, S. Kühl, C. Rettenmaier, M. Lopez Luna, F. T. Haase and B. Roldan Cuenya, Operando Investigation of Ag-Decorated Cu_2O Nanocube Catalysts with Enhanced CO_2 Electroreduction toward Liquid Products, *Angew. Chem., Int. Ed.*, 2021, **60**, 7426–7435.
20 J. De Ruiter, H. An, L. Wu, Z. Gijsberg, S. Yang, T. Hartman, B. M. Weckhuysen and W. Van Der Stam, Probing the

Dynamics of Low-Overpotential CO_2-to-CO Activation on Copper Electrodes with Time-Resolved Raman Spectroscopy, *J. Am. Chem. Soc.*, 2022, **144**, 15047–15058.

21 A. Posada-Borbón and H. Grönbeck, A First-Principles-Based Microkinetic Study of CO_2 Reduction to CH_3OH over In_2O_3(110), *ACS Catal.*, 2021, **11**, 9996–10006.

22 S. Sun, M. D. Higham, X. Zhang and C. R. A. Catlow, Multiscale Investigation of the Mechanism and Selectivity of CO_2 Hydrogenation over Rh(111), *ACS Catal.*, 2024, **14**, 5503–5519.

23 I. Kowalec, L. Kabalan, C. R. A. Catlow and A. J. Logsdail, A computational study of direct CO_2 hydrogenation to methanol on Pd surfaces, *Phys. Chem. Chem. Phys.*, 2022, **24**, 9360–9373.

24 Y. Yang, M. G. White and P. Liu, Theoretical study of methanol synthesis from CO_2 hydrogenation on metal-doped Cu(111) surfaces, *J. Phys. Chem. C*, 2012, **116**, 248–256.

25 F. Cannizzaro, S. Kurstjens, T. van den Berg, E. J. M. Hensen and I. A. W. Filot, A computational study of CO_2 hydrogenation on single atoms of Pt, Pd, Ni and Rh on In_2O_3(111), *Catal. Sci. Technol.*, 2023, **13**, 4701–4715.

26 A. H. Motagamwala and J. A. Dumesic, Microkinetic Modeling: A Tool for Rational Catalyst Design, *Chem. Rev.*, 2021, **121**, 1049–1076.

27 S. R. Kulkarni, G. Lezcano, V. K. Velisoju, N. Realpe and P. Castaño, Microkinetic Modeling to Decode Catalytic Reactions and Empower Catalytic Design, *ChemCatChem*, 2024, **16**, e202301720.

28 S. Morandi, O. Loveday, T. Renningholtz, S. Pablo-García, R. A. Vargas-Hernández, R. R. Seemakurthi, P. S. Berman, R. García-Muelas, A. Aspuru-Guzik and N. López, A Foundational Model for Reaction Networks on Metal Surfaces, *ChemRxiv*, 2024, DOI: 10.26434/CHEMRXIV-2024-BFV3D.

29 Y. Ureel, L. Tomme, M. K. Sabbe and K. M. Van Geem, Genesys-Cat: automatic microkinetic model generation for heterogeneous catalysis with improved Bayesian optimization, *Catal. Sci. Technol.*, 2025, **15**, 750–764.

30 O. Schilter, A. Vaucher, P. Schwaller and T. Laino, Designing catalysts with deep generative models and computational data. A case study for Suzuki cross coupling reactions, *Digital Discovery*, 2023, **2**, 728–735.

31 F. Göltl, M. Mavrikakis, F. Göltl and M. Mavrikakis, Generalized Brønsted-Evans-Polanyi Relationships for Reactions on Metal Surfaces from Machine Learning, *ChemCatChem*, 2022, **14**, e202201108.

32 D. J. Hutton, K. E. Cordes, C. Michel and F. Göltl, Machine Learning-Based Prediction of Activation Energies for Chemical Reactions on Metal Surfaces, *J. Chem. Inf. Model.*, 2023, **63**, 6006–6013.

33 K. Lee, M. Kim and H. Kim, Catalytic nanoparticles being facet-controlled, *J. Mater. Chem.*, 2010, **20**, 3791–3798.

34 M. B. Gawande, A. Goswami, F. X. Felpin, T. Asefa, X. Huang, R. Silva, X. Zou, R. Zboril and R. S. Varma, Cu and Cu-Based Nanoparticles: Synthesis and Applications in Catalysis, *Chem. Rev.*, 2016, **116**, 3722–3811.

35 S. Cai, D. Wang, Z. Niu and Y. Li, Progress in organic reactions catalyzed by bimetallic nanomaterials, *Chin. J. Catal.*, 2013, **34**, 1964–1974.

36 S. Mitchell, R. Qin, N. Zheng and J. Pérez-Ramírez, Nanoscale engineering of catalytic materials for sustainable technologies, *Nat. Nanotechnol.*, 2020, **16**, 129–139.

37 V. Fung, G. Hu, Z. Wu and D. E. Jiang, Hydrogen in Nanocatalysis, *J. Phys. Chem. Lett.*, 2020, **11**, 7049–7057.

38 G. Peng and M. Mavrikakis, Adsorbate diffusion on transition metal nanoparticles, *Nano Lett.*, 2015, **15**, 629–634.

39 S. Saini, J. Halldin Stenlid and F. Abild-Pedersen, Electronic structure factors and the importance of adsorbate effects in chemisorption on surface alloys, *npj Comput. Mater.*, 2022, **8**, 1–12.

40 K. Gu and S. Lin, Advances in the Dynamics of Adsorbate Diffusion on Metal Surfaces: Focus on Hydrogen and Oxygen, *ChemPhysChem*, 2024, **25**, e202400083.

41 S. Gu, Z. Yang, J. Ding, J. Li, L. Wang, H. Wan and G. Guan, Mechanism investigation on the synergistic effect between Fe_5C_2 and Cu in CuFeZn catalysts for the selective hydrogenation of CO_2 to ethanol, *Appl. Catal., A*, 2025, **704**, 120375.

42 A. M. Verma, S. Chaturvedi, S. Paul, S. Nandi, R. Sheshanarayana, K. Santhosh, G. Valavarasu, A. Dukkipati, G. G. Chuandayani, Y. M. Pei, C. Q. J. Ng, A. Amrute and A. G. Rajan, Data-driven massive reaction networks reveal new pathways underlying catalytic CO_2 hydrogenation, *ChemRxiv*, 2025, DOI: 10.26434/chemrxiv-2025-pnh6l.

43 B. Ni and X. Wang, Face the Edges: Catalytic Active Sites of Nanomaterials, *Adv. Sci.*, 2015, **2**, 1500085.

44 Y. Gao, S. Liu, Z. Zhao, H. Tao and Z. Sun, Heterogeneous Catalysis of CO_2 Hydrogenation to C^{2+} Products, *Acta Phisico-Chim. Sin.*, 2018, **34**, 858–872.

45 C. Panzone, R. Philippe, C. Nikitine, A. Bengaouer, A. Chappaz and P. Fongarland, Development and Validation of a Detailed Microkinetic Model for the CO_2 Hydrogenation Reaction toward Hydrocarbons over an Fe–K/Al_2O_3 Catalyst, *Ind. Eng. Chem. Res.*, 2022, **61**, 4514–4533.

46 Y. Jiang, R. Long and Y. Xiong, Regulating C–C coupling in thermocatalytic and electrocatalytic COx conversion based on surface science, *Chem. Sci.*, 2019, **10**, 7310–7326.

47 B. Kreitz, K. Sargsyan, K. Blöndal, E. J. Mazeau, R. H. West, G. D. Wehinger, T. Turek and C. F. Goldsmith, Quantifying the Impact of Parametric Uncertainty on Automatic Mechanism Generation for CO_2 Hydrogenation on Ni(111), *JACS Au*, 2021, **1**, 1656–1673.

48 B. Kreitz, P. Lott, F. Studt, A. J. Medford, O. Deutschmann and C. F. Goldsmith, Automated Generation of Microkinetics for Heterogeneously Catalyzed Reactions Considering Correlated Uncertainties, *Angew. Chem., Int. Ed.*, 2023, **62**, e202306514.

49 Y. F. Shi, S. Ma and Z. P. Liu, Copper-based catalysts for CO_2 hydrogenation: a perspective on active sites, *EES Catal.*, 2023, **1**, 921–933.

50 B. Zijlstra, R. J. P. Broos, W. Chen, G. L. Bezemer, I. A. W. Filot and E. J. M. Hensen, The Vital Role of Step-

Edge Sites for Both CO Activation and Chain Growth on Cobalt Fischer–Tropsch Catalysts Revealed through First-Principles-Based Microkinetic Modeling Including Lateral Interactions, *ACS Catal.*, 2020, **10**, 9376–9400.

51 C. Vogt and B. M. Weckhuysen, The concept of active site in heterogeneous catalysis, *Nat. Rev. Chem.*, 2022, **6**, 89–111.

52 R. Svensson and H. Grönbeck, Site Communication in Direct Formation of H_2O_2 over Single-Atom Pd@Au Nanoparticles, *J. Am. Chem. Soc.*, 2023, **145**, 11579–11588.

53 Z. Bin Ding and M. Maestri, Development and Assessment of a Criterion for the Application of Brønsted–Evans–Polanyi Relations for Dissociation Catalytic Reactions at Surfaces, *Ind. Eng. Chem. Res.*, 2019, **58**, 9864–9874.

54 R. P. Ye, J. Ding, W. Gong, M. D. Argyle, Q. Zhong, Y. Wang, C. K. Russell, Z. Xu, A. G. Russell, Q. Li, M. Fan and Y. G. Yao, CO_2 hydrogenation to high-value products via heterogeneous catalysis, *Nat. Commun.*, 2019, **10**, 1–15.

55 R. Kas, R. Kortlever, A. Milbrat, M. T. M. Koper, G. Mul and J. Baltrusaitis, Electrochemical CO_2 reduction on Cu_2O-derived copper nanoparticles: controlling the catalytic selectivity of hydrocarbons, *Phys. Chem. Chem. Phys.*, 2014, **16**, 12194–12201.

56 H. Xie, T. Wang, J. Liang, Q. Li and S. Sun, Cu-based nanocatalysts for electrochemical reduction of CO_2, *Nano Today*, 2018, **21**, 41–54.

57 M. Irshad, H. J. Chun, M. K. Khan, H. Jo, S. K. Kim and J. Kim, Synthesis of *n*-butanol-rich C^{3+} alcohols by direct CO_2 hydrogenation over a stable Cu–Co tandem catalyst, *Appl. Catal., B*, 2024, **340**, 123201.

58 D. Xu, M. Ding, X. Hong, G. Liu and S. C. E. Tsang, Selective C^{2+} Alcohol Synthesis from Direct CO_2 Hydrogenation over a Cs-Promoted Cu-Fe-Zn Catalyst, *ACS Catal.*, 2020, **10**, 5250–5260.

59 T. Liu, D. Xu, M. Song, X. Hong and G. Liu, K–ZrO_2 Interfaces Boost CO_2 Hydrogenation to Higher Alcohols, *ACS Catal.*, 2023, **13**, 4667–4674.

60 C. Yang, S. Liu, Y. Wang, J. Song, G. Wang, S. Wang, Z.-J. Zhao, R. Mu and J. Gong, The Interplay between Structure and Product Selectivity of CO_2 Hydrogenation, *Angew. Chem., Int. Ed.*, 2019, **58**(33), 11242–11247.

61 H. Guo, S. Li, F. Peng, H. Zhang, L. Xiong, C. Huang, C. Wang and X. Chen, Roles Investigation of Promoters in K/Cu–Zn Catalyst and Higher Alcohols Synthesis from CO_2 Hydrogenation over a Novel Two-Stage Bed Catalyst Combination System, *Catal. Lett.*, 2015, **145**, 620–630.

62 A. Reina, T. Dang-Bao, I. Guerrero-Ríos and M. Gómez, Palladium and Copper: Advantageous Nanocatalysts for Multi-Step Transformations, *Nanomaterials*, 2021, **11**, 1891.

63 B. R. Karimadom, A. Sermiagin, D. Meyerstein, T. Zidki, A. Mizrahi, R. Bar-Ziv and H. Kornweitz, Hydrogen adsorption on various transition metal (111) surfaces in water: a DFT forecast, *Phys. Chem. Chem. Phys.*, 2024, **26**, 7647–7657.

64 C. Yang, R. Mu, G. Wang, J. Song, H. Tian, Z. J. Zhao and J. Gong, Hydroxyl-mediated ethanol selectivity of CO_2 hydrogenation, *Chem. Sci.*, 2019, **10**, 3161–3167.

65 R. P. Ye, J. Ding, W. Gong, M. D. Argyle, Q. Zhong, Y. Wang, C. K. Russell, Z. Xu, A. G. Russell, Q. Li, M. Fan and Y. G. Yao, CO_2 hydrogenation to high-value products via heterogeneous catalysis, *Nat. Commun.*, 2019, **10**, 5698.

66 Y. Chen, J. Liu, X. Chen, S. Gu, Y. Wei, L. Wang, H. Wan and G. Guan, Development of Multifunctional Catalysts for the Direct Hydrogenation of Carbon Dioxide to Higher Alcohols, *Molecules*, 2024, **29**, 2666.

67 G. Cui, Y. Lou, M. Zhou, Y. Li, G. Jiang and C. Xu, Review of Mechanism Investigations and Catalyst Developments for CO_2 Hydrogenation to Alcohols, *Catalysts*, 2024, **14**, 232.

68 M. Behrens, F. Studt, I. Kasatkin, S. Kühl, M. Hävecker, F. Abild-Pedersen, S. Zander, F. Girgsdies, P. Kurr, B. L. Kniep, M. Tovar, R. W. Fischer, J. K. Nørskov and R. Schlögl, The Active Site of Methanol Synthesis over $Cu/ZnO/Al_2O_3$ Industrial Catalysts, *Science*, 2012, **336**, 893–897.

69 S. Kattel, P. J. Ramírez, J. G. Chen, J. A. Rodriguez and P. Liu, Active sites for CO_2 hydrogenation to methanol on Cu/ZnO catalysts, *Science*, 2017, **355**, 1296–1299.

70 R. M. Palomino, P. J. Ramírez, Z. Liu, R. Hamlyn, I. Waluyo, M. Mahapatra, I. Orozco, A. Hunt, J. P. Simonovis, S. D. Senanayake and J. A. Rodriguez, Hydrogenation of CO_2 on ZnO/Cu(100) and ZnO/Cu(111) Catalysts: Role of Copper Structure and Metal–Oxide Interface in Methanol Synthesis, *J. Phys. Chem. B*, 2017, **122**, 794–800.

71 B. Hu, Y. Yin, G. Liu, S. Chen, X. Hong and S. C. E. Tsang, Hydrogen spillover enabled active Cu sites for methanol synthesis from CO_2 hydrogenation over Pd doped CuZn catalysts, *J. Catal.*, 2018, **359**, 17–26.

72 L. C. Grabow and M. Mavrikakis, Mechanism of methanol synthesis on cu through CO_2 and CO hydrogenation, *ACS Catal.*, 2011, **1**, 365–384.

73 J. Zhao, Y. Song, M. Eswaran, F. Buendia-Zamudio and S. M. Kozlov, Active Phase of Cu-ZnO Catalysts in Methanol Synthesis, *J. Energy Chem.*, 2026, DOI: 10.1016/j.jechem.2026.01.053.

74 X. Nie, X. Ren, C. Tu, C. Song, X. Guo and J. G. Chen, Computational and experimental identification of strong synergy of the Fe/ZnO catalyst in promoting acetic acid synthesis from CH_4 and CO_2, *Chem. Commun.*, 2020, **56**, 3983–3986.

75 M. G. Sibi, D. Verma, H. C. Setiyadi, M. K. Khan, N. Karanwal, S. K. Kwak, K. Y. Chung, J. H. Park, D. Han, K. W. Nam and J. Kim, Synthesis of monocarboxylic acids via direct CO_2 conversion over Ni–Zn intermetallic catalysts, *ACS Catal.*, 2021, **11**, 8382–8398.

76 Z. He, M. Cui, Q. Qian, J. Zhang, H. Liu and B. Han, Synthesis of liquid fuel via direct hydrogenation of CO_2, *Proc. Natl. Acad. Sci. U. S. A.*, 2019, **116**, 12654–12659.

77 C. Tu, X. Nie and J. G. Chen, Insight into Acetic Acid Synthesis from the Reaction of CH_4 and CO_2, *ACS Catal.*, 2021, 3384–3401.

78 W. Chen, I. A. W. Filot, R. Pestman and E. J. M. Hensen, Mechanism of Cobalt-Catalyzed CO Hydrogenation: 2. Fischer-Tropsch Synthesis, *ACS Catal.*, 2017, **7**, 8061–8071.

79 W. Chen, T. F. Kimpel, Y. Song, F. K. Chiang, B. Zijlstra, R. Pestman, P. Wang and E. J. M. Hensen, Influence of Carbon Deposits on the Cobalt-Catalyzed Fischer-Tropsch Reaction: Evidence of a Two-Site Reaction Model, *ACS Catal.*, 2018, **8**, 1580–1590.
80 S. M. Kozlov, F. Viñes and A. Görling, Bonding mechanisms of graphene on metal surfaces, *J. Phys. Chem. C*, 2012, **116**, 7360–7366.
81 M. G. Evans and M. Polanyi, Some applications of the transition state method to the calculation of reaction velocities, especially in solution, *Trans. Faraday Soc.*, 1935, **31**, 875–894.
82 A. Vojvodic, F. Calle-Vallejo, W. Guo, S. Wang, A. Toftelund, F. Studt, J. I. Martínez, J. Shen, I. C. Man, J. Rossmeisl, T. Bligaard, J. K. Nrskov and F. Abild-Pedersen, On the behavior of Brønsted–Evans–Polanyi relations for transition metal oxides, *J. Chem. Phys.*, 2011, **134**, 244509.
83 R. Alcalá, M. Mavrikakis and J. A. Dumesic, DFT studies for cleavage of C–C and C–O bonds in surface species derived from ethanol on Pt(111), *J. Catal.*, 2003, **218**, 178–190.
84 S. Wang, B. Temel, J. Shen, G. Jones, L. C. Grabow, F. Studt, T. Bligaard, F. Abild-Pedersen, C. H. Christensen and J. K. Nørskov, Universal Brønsted–Evans–Polanyi relations for C–C, C–O, C–N, N–O, N–N, and O–O dissociation reactions, *Catal. Lett.*, 2011, **141**, 370–373.
85 S. Wang, V. Vorotnikov, J. E. Sutton and D. G. Vlachos, Brønsted-evans-polanyi and transition state scaling relations of furan derivatives on Pd(111) and their relation to those of small molecules, *ACS Catal.*, 2014, **4**, 604–612.
86 L. Goerigk, A. Hansen, C. Bauer, S. Ehrlich, A. Najibi and S. Grimme, A look at the density functional theory zoo with the advanced GMTKN55 database for general main group thermochemistry, kinetics and noncovalent interactions, *Phys. Chem. Chem. Phys.*, 2017, **19**, 32184–32215.
87 N. T. Anh, O. Eisenstein, J. M. Lefour and M. E. T. H. Dàu, Orbital Factors and Asymmetric Induction, *J. Am. Chem. Soc.*, 1973, **95**, 6146–6147.
88 S. Wang, V. Petzold, V. Tripkovic, J. Kleis, J. G. Howalt, E. Skúlason, E. M. Fernández, B. Hvolbæk, G. Jones, A. Toftelund, H. Falsig, M. Björketun, F. Studt, F. Abild-Pedersen, J. Rossmeisl, J. K. Nørskov and T. Bligaard, Universal transition state scaling relations for (de)hydrogenation over transition metals, *Phys. Chem. Chem. Phys.*, 2011, **13**, 20760–20765.
89 J. K. Nørskov, T. Bligaard, B. Hvolbæk, F. Abild-Pedersen, I. Chorkendorff and C. H. Christensen, The nature of the active site in heterogeneous metal catalysis, *Chem. Soc. Rev.*, 2008, **37**, 2163–2171.
90 M. B. Smith and J. March, *March's Advanced Organic Chemistry*, John Wiley & Sons, Inc., Hoboken, NJ, USA, 2006.
91 M. V. Polynski, S. M. Kozlov and C. Authors, Construction of Sabatier Volcanoes for CO_2 Hydrogenation to C_{1-2} Oxygenates Using Data-Efficient Machine Learning, *ChemRxiv*, 2025, DOI: 10.26434/CHEMRXIV-2025-5W31T.
92 L. Falivene, S. M. Kozlov and L. Cavallo, Constructing Bridges between Computational Tools in Heterogeneous and Homogeneous Catalysis, *ACS Catal.*, 2018, **8**, 5637–5656.
93 Z. W. She, J. Kibsgaard, C. F. Dickens, I. Chorkendorff, J. K. Nørskov and T. F. Jaramillo, Combining theory and experiment in electrocatalysis: insights into materials design, *Science*, 2017, **355**, eaad4998.
94 X. Ding, J. Fu, Y. Lyu, L. Ma, Y. Xu and X. Liu, Active sites of the cobalt catalysts controlled by surface silanols of silicalite-1 in CO_2 hydrogenation to ethanol, *Chem. Eng. J.*, 2024, **494**, 152923.
95 Y. Zhang and W. Yang, Comment on "Generalized Gradient Approximation Made Simple", *Phys. Rev. Lett.*, 1998, **80**, 890.
96 G. Kresse and D. Joubert, From ultrasoft pseudopotentials to the projector augmented-wave method, *Phys. Rev. B: Condens. Matter Mater. Phys.*, 1999, **59**, 1758–1775.
97 S. Grimme, J. Antony, S. Ehrlich and H. Krieg, A consistent and accurate ab initio parametrization of density functional dispersion correction (DFT-D) for the 94 elements H-Pu, *J. Chem. Phys.*, 2010, **132**, 154104.
98 S. Grimme, S. Ehrlich and L. Goerigk, Effect of the damping function in dispersion corrected density functional theory, *J. Comput. Chem.*, 2011, **32**, 1456–1465.
99 S. Grimme, C. Bannwarth and P. Shushkov, A Robust and Accurate Tight-Binding Quantum Chemical Method for Structures, Vibrational Frequencies, and Noncovalent Interactions of Large Molecular Systems Parametrized for All spd-Block Elements (Z = 1–86), *J. Chem. Theory Comput.*, 2017, **13**, 1989–2009.
100 A. Hjorth Larsen, J. JØrgen Mortensen, J. Blomqvist, I. E. Castelli, R. Christensen, M. Dułak, J. Friis, M. N. Groves, B. Hammer, C. Hargus, E. D. Hermes, P. C. Jennings, P. Bjerre Jensen, J. Kermode, J. R. Kitchin, E. Leonhard Kolsbjerg, J. Kubal, K. Kaasbjerg, S. Lysgaard, J. Bergmann Maronsson, T. Maxson, T. Olsen, L. Pastewka, A. Peterson, C. Rostgaard, J. SchiØtz, O. Schütt, M. Strange, K. S. Thygesen, T. Vegge, L. Vilhelmsen, M. Walter, Z. Zeng and K. W. Jacobsen, The atomic simulation environment—a Python library for working with atoms, *J. Phys.: Condens. Matter*, 2017, **29**, 273002.
101 S. M. Kozlov, H. A. Aleksandrov and K. M. Neyman, Energetic Stability of Absorbed H in Pd and Pt Nanoparticles in a More Realistic Environment, *J. Phys. Chem. C*, 2015, **119**, 5180–5186.
102 J. Chen, M. Aliasgar, Y. Zhao, F. B. Zamudio, L. Fan, J. Chen, J. Chen, X. Gu, J. Gao, S. M. Kozlov and L. Wang, Unlocking cathodic potential dependent Pd deactivation for energy efficient CO_2 electroreduction to formate, *Nat. Commun.*, 2025, **16**, 10169.
103 D. Leybo, U. J. Etim, M. Monai, S. R. Bare, Z. Zhong and C. Vogt, Metal–support interactions in metal oxide-supported atomic, cluster, and nanoparticle catalysis, *Chem. Soc. Rev.*, 2024, **53**, 10450–10490.
104 F. Buendia-Zamudio, J. Zhao, J. Bahodurov and S. M. Kozlov, Nanoeffects in the Design of Catalysts for Green Energy Technologies, *under revision*, 2026.
105 M. V. Polynski and S. M. Kozlov, Reaction_network_exploration_tools (GitHub repository), https://github.com/Computational-Nanocatalysis-Group/Reaction_network_exploration_tools, (accessed 6 February 2026).